FRIGID ZONE **MEDICINE**
Review • DOI: 10.1515/fzm-2025-0010

Rewarming strategies for cryopreservation: Technological challenges and opportunities in energy conversion

Ruidong Ma[1], Ziyuan Wang[1], Ren Shen[1,2], Zhiquan Shu[1,3], Chen Ming[1], Dayong Gao[1]

Abstract

Cryopreservation of living cells and tissues plays a vital role in biomedical research, clinical applications, biotechnology innovation, the development of new vaccines and drugs, and the conservation of endangered species. While significant technological breakthroughs have been achieved in cooling methods—particularly through vitrification for large tissue and organs—the lack of optimal rewarming technology remains a key obstacle to successful cryopreservation, especially for larger samples such as tissues and organs. The primary challenges during the warming process include non-uniformity heating and insufficient rewarming rates, which can lead to thermal stress-induced structural damage and lethal ice recrystallization, ultimately compromising the integrity and functionality of biological materials. In recent years, various advanced warming techniques have emerged, employing different energy conversion approaches to achieve volumetric heating while minimizing the risk of overheating. These techniques involve thermal, mechanical-thermal, and electromagnetic-thermal energy conversions. However, each method presents its own limitation. This review aims to summarize recent advancements in rewarming technologies for cryopreservation, with a focus on their mechanisms, applications, and the key challenges that must be addressed to enable broader adoption in medical and commercial contexts.

Keywords

cryopreservation; rewarming technology; energy conservation; electromagnetic

Received 14 January 2025, accepted 07 April 2025

[1]*Department of Mechanical Engineering, University of Washington, Seattle 98195, USA*
[2]*Department of Mechanical Engineering, Seattle University, Seattle 98122, USA*
[3]*School of Engineering and Technology, University of Washington Tacoma, Tacoma 98402, USA*

**Corresponding author Dayong Gao, E-mail: dayong@uw.edu*

1 Introduction

In 1949, Polge accidently discovered that glycerol has a cryoprotective properties that protect sperm during freezing[1]. Since then, sub-zero temperature technologies have been widely applied not only for destroying cancerous tumors through cryoablation, but also for preserving living biospecimens. Thanks to technological advances over the past century, cryopreservation has found applications in diverse fields, including reproduction[2-3]. Since then, sub-zero temperature technologies have been widely applied not only for destroying cancerous tumors through cryoablation, but also for preserving living biospecimens. Thanks to technological advances over the past century, cryopreservation has found applications in diverse fields, including reproduction[2-3], the preservation of endangered species[4-6], clinical medicine[7-9], and fundamental research[10-13].

Cryopreservation was initially developed as a tool in animal reproduction, facilitating genetic selection and breeding in species such as cows and Kurobuta pork, particularly during widespread infectious disease outbreaks[14]. It also plays a critical role in preserving the germ cells of endangered animals and seeds of rare plants in global biobanks. Currently, more than 120 such biobanks operate worldwide under the coordination of the International Society for Biological and Environmental Repositories (ISBER)[4,15]. In 2024, ISBER launched a special interest group dedicated to advancing cryopreservation science. In clinical settings, cryopreservation is essential in advanced cellular therapies[12,16], blood transfusion services[17-18], and vaccination development[19]. The ability to store sperm and oocytes also

benefits patients with infertility due to either genetic or environmental causes. In basic research, cryopreservation provides a long-term storage strategy for living biological samples, which is critical for pharmaceutical development and the study of complex biological systems such as organoids[20]. Although specific cryopreservation methods and regulatory considerations vary by sample type, most protocols follow a general workflow, as illustrated in Fig. 1A. This process typically includes sample collection, the addition of Cryoprotective Agents (CPAs), cooling or vitrification, storage, and thawing. After thawing, samples are evaluated before being put to use.

The principle of cryopreservation is to use low temperatures to reduce the biological and chemical reaction rate in biological samples, thereby extending their preservation time. In 1972, Mazur proposed the "Two-factor hypothesis" of freezing injury, inspired by research on Chinese hamster tissue[21]. As shown in Fig. 1B, this hypothesis describes two primary mechanisms of cryoinjury. When a sample is cooled below its freezing point, ice crystals begin to form and grow in the extracellular space[22]. The plasma membrane serves as a barrier, preventing these extracellular ice crystals from entering the cell. Meanwhile, macromolecules inside the cell help maintain in a supercooled state[23]. However, if the cooling rate is too fast, the supercooled state may be disrupted, leading to Intracellular Ice Formation (IIF). IIF can rupture cell membranes and result in cell death[24]. Conversely, excessively slow cooling allows more water to leave the cell, reducing the likelihood of IIF, but causes the intracellular environment to become hypertonic, leading to cellular dehydration due to the "solution effect". Both IIF and solution effect-induced dehydration are fatal to cells. Therefore, an optimal, cell-type-specific cooling rate is necessary to avoid both extremes.

Subsequent studies demonstrated that rapid rewarming can improve post-thaw recovery[23-25]. While rapid cooling may induce the formation of small intracellular ice crystals can remain thermodynamically unstable. During slow rewarming, these crystals may recrystallize-melting and then refreezing into larger, more damaging crystals-causing cell death[26]. Interestingly, cells subjected to suboptimal cooling rates can sometimes survive if they are rewarmed rapidly enough, further highlighting the importance of rewarming rates.

Vitrification, a technique used to bypass ice crystal formation altogether, achieves an amorphous, glass-like state and is widely discussed in polymer science[27-29]. Since tissues and organs contain diverse cell types with varying optimal cooling rates, vitrification offers a viable strategy for cryopreserving large biological systems by avoiding ice formation entirely. This process requires a minimum cooling rate known as the *Critical Cooling Rate* (CCR). For pure water or isotonic solutions, the CCR can be as high as 10^6 °C/min[10], making it technically challenging. However, the inclusion of CPAs and large molecular weight polymers can reduce the required CCR to approximately 10 °C/min or lower[30].

Despite these advances, vitrified samples still face the risk of lethal ice recrystallization during rewarming. The minimum rewarming rate required to prevent recrystallization is known as the Critical Warming Rate (CWR). Hence, successful cryopreservation depends not only on efficient cooling but also on rapid

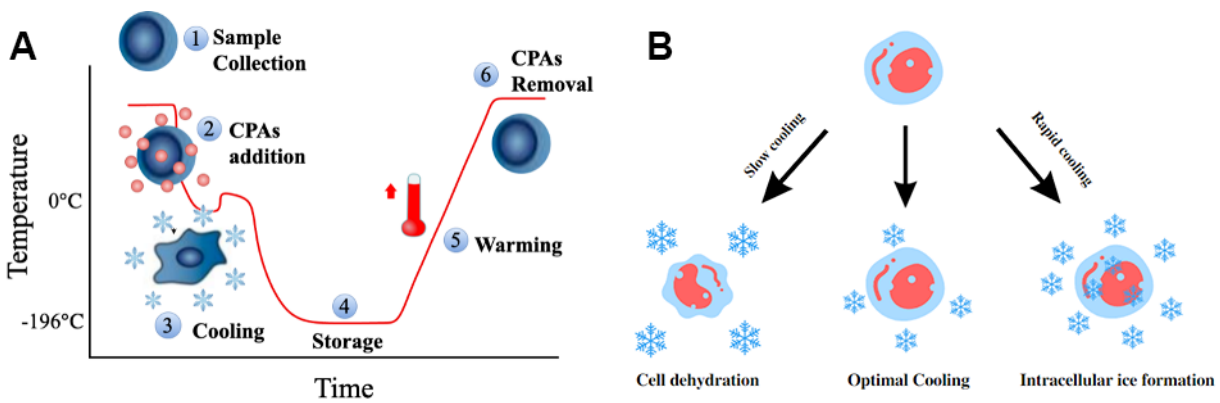

Fig. 1 Cryopreservation standard procedures and Peter Mazur's "two-factor" hypothesis

(A) Major steps of cryopreservation. The sample temperature is initially lowered to 0 °C to allow for the addition of cryoprotective agents (CPAs), followed by further cooling to reach the target cryogenic temperature. Storage requires proper moisture control and maintenance of a stable low temperature. Rewarming then returns the sample from ultra-low temperatures to 0 °C, after which CPAs are removed. Finally, sample functionality and metabolic activity are assessed before future application. (B) Peter Mazur's "Two-factor" Hypothesis. During slow cooling, cells undergo dehydration due to the solution effect. Conversely, rapid cooling can lead to intracellular ice formation, which is lethal to cells. Therefore, an optimal, cell-type-specific cooling rate is required to avoid both intracellular ice formation and excessive dehydration.

and uniform rewarming. Uneven temperature distribution can lead to mechanical stress, resulting in fractures in brittle, frozen tissues—particularly problematic in large samples[31-35].

While small-volume cryopreservation (*e.g.*, under 2 mL of stem cells) is routinely successful, cryopreserving large-volume systems—such as bulk cell suspensions, tissues, or whole organs—remains a major challenge due to ice crystal formation and poor thermal control[27,36]. This technical limitation severely restricts clinical and research applications. In the United States alone, nearly 110,000 people were on the national organ transplant waiting list in 2021, with over 40000 transplants performed in 2020. Despite this, approximately 17 people die each day due to a shortage of matched organs[37]. Organ preservation technologies, such as normothermic and hypothermic machine perfusion, can currently extend viability for only up to 24 hours. As a result, around 28000 donated organs are wasted annually due to insufficient preservation time[38].

If organ cryopreservation becomes technically feasible, it could revolutionize the field—facilitating organ matching, transportation, and transplantation, while also supporting advances in gene therapy and tissue engineering. Thus, there is an urgent need to scale up cryopreservation techniques for larger biological samples.

Overall, cryopreservation remains one of the most promising technologies for long-term biological sample storage[39-40]. Advances in vitrification[27] and understanding of critical cooling rates[16] help mitigate the risks of IIF and cellular dehydration[21,29]. Nevertheless, rapid and uniform rewarming remains a critical bottleneck in cryopreservation. Rewarming requires much higher rates than cooling and must avoid thermal gradients, posing substantial engineering and energy conversion challenges.

In response, recent research has focused on developing efficient energy conversion techniques for rewarming cryopreserved biomaterials. In this review, we highlight and compare various rewarming methods based on different energy conversion or transfer mechanisms: thermal-to-thermal (*e.g.*, water bath and forced air heating), mechanical-to-thermal (*e.g.*, ultrasound-induced heating[41-42]), and electromagnetic-to-thermal. The latter category includes laser[43-45], electric field[46-50], and magnetic field[51-53] heating technologies. Electric field heating comprises methods such as Joule heating, capacitor heating, antenna heating, and cavity heating, spanning operational frequencies from hertz to megahertz. Magnetic heating is typically based on induction, involving eddy currents and magnetic hysteresis. These various energy conversion strategies are summarized in Fig. 2, illustrating their principles and applications in cryopreservation rewarming.

2 Energy sources, heating mechanisms, and applications

2.1 Thermal energy source

When using thermal energy to rewarm cryopreserved samples, traditional methods rely on conduction or convection heat transfer mechanisms. These approaches depend on the temperature gradient between the heating source and the cryopreserved biomaterials to drive heat diffusion. However, such gradients often lead to non-uniform rewarming and the development of thermal stress within the sample. Over the past decades, researchers have developed and refined a variety of conduction and convection-based rewarming devices. These advancements aim to improve rewarming rates, prevent ice recrystallization, ensure temperature uniformity, and reduce the risk of overheating the outer layers during the thawing process.

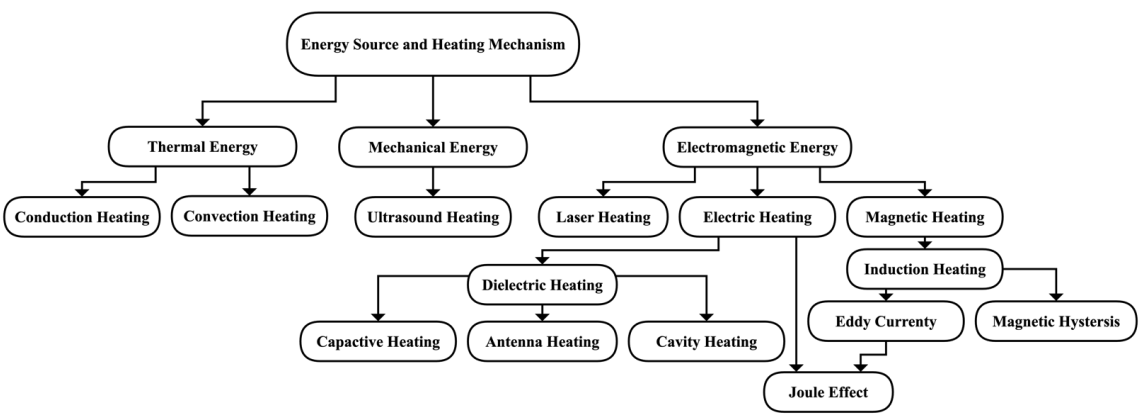

Fig. 2 Energy conversion sources and methods used in cryopreservation rewarming technologies

Three primary categories of energy sources-thermal, mechanical, and electromagnetic-are employed to achieve rapid and uniform heating. Each category involves distinct heating mechanisms and has specific applications in cryopreservation rewarming.

2.2 Conduction heating

Conduction heat transfer occurs when there is a temperature gradient between two objects and the intermediate medium is a solid or a stationary fluid, such as a liquid or gas. In cryopreservation, conduction heating is often referred to as a water-free rewarming method. In 2002, a semi-automatic dry thawing device was developed by Saharda, Tansmed, Germany, using two heating chambers and applied to the investigations of leukapheresis products[54]. In this system, one chamber warms designed to conform to the sample bags, while the other chamber includes a heated metal plate and an infrared temperature senso. The reported rewarming duration was 3-5 min; however, the specific rewarming rate was not provided. Subsequently, progenitor cells (100-140 mL) were successfully cryopreserved and rewarmed using a dry thawing device, achieving a rewarming rate of approximately 2.58 °C/min and demonstrating comparable viability to that obtained with traditional water bath thawing. This method is considered preferable due to its reduced risk of contamination[18]. More recently, leukapheresis cell products (ranging from 60-140 mL) were rewarmed using a controlled-rate thawing station (VIAThaw, Cytiva, Cambridge, UK), which utilizes two heated metal plates set at 34 °C to warm the cryobag simultaneously from the top and bottom surfaces[55]. Fig. 3A presentsa schematic illustration of the dry thawing device. The dual hot plates heat the sample surfaces, and thermal energy is transferred into the interior *via* conduction. The heat flux during conduction-based rewarming can be described by Fourier's law.

$$q'' = -k_x \frac{\partial T}{\partial x} - k_y \frac{\partial T}{\partial y} - k_z \frac{\partial T}{\partial z}$$

Where T is temperature; x, y, and z are the three-dimension in cartesian coordinates; kx, ky, and kz are the thermal conductivities in x, y, and z directions, respectively.

2.3 Convection heating

Convection heat transfer occurs when a high-temperature fluid, either liquid or gas, moves over cryopreserved samples. This process is governed by Newton's law of cooling, which states:

$$q'' = h(T_s - T_\infty)$$

Where q'' represents heat flux W/m^2, T_s is cryopreserved sample temperature, T_∞ is hot fluid temperature, and h is convective heat transfer coefficient.

The water bath serves as the gold standard in current clinical usage for rewarming low-temperature materials, relying on convection heat transfer between the liquid (mainly 37 °C water) and the sample container, as shown in Fig. 3B. For samples under the conventional cooling method, the outer layer of solid ice first melts and turns into liquid water due to the high thermal gradient between the source and the sample. Since ice has a larger thermal conductivity (k) of 8 W/m °C[56] and lower heat capacity (C) of 700 J/°C kg[57] at -193 °C, compared to liquid water, which has a thermal conductivity of 0.56 W/m °C and heat capacity of 4217 J/°C kg at 0 °C[58], both the thermal resistance and the energy required to raise the temperature per degree increase. This transition from a good thermal conductor (ice) to a poor thermal conductor (liquid water) reduces the thawing rate. For successfully vitrified samples, water baths are unable to achieve the CWR necessary to prevent ice recrystallization during thawing[59]. In both scenarios, high temperature gradients between the outer surface and the core generate substantial thermal stress, which can lead to cracking[32]. Therefore,

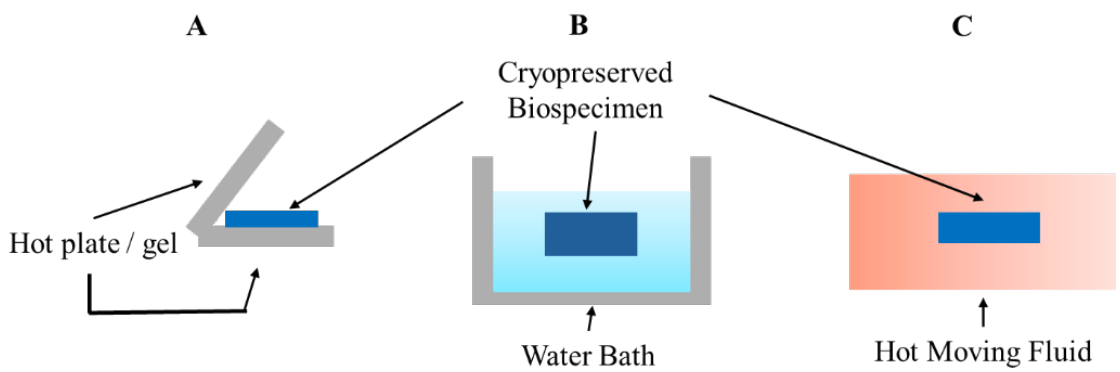

Fig. 3 Illustration of the conventional heating method in cryopreservation

(A) Dry thawing utilizing a conduction heat transfer mechanism, where heated plates warm the sample *via* direct contact. (B) Water bath rewarming, where the sample is immersed in warm water to enable heat transfer through conduction and convection. (C) Hot moving fluid rewarming (typically heated air), demonstrating a convection heat transfer mechanism from left to right.

although the water bath is the cheapest and most convenient thawing approach, it still presents some unavoidable and fatal challenges[60]. Table 1 illustrates some representative rewarming experiments using water bath for various sample types and volumes. Smaller samples have higher rewarming rates and less temperature gradient due to spatial effects. As the sample size increases, the thawing rate significantly decreases. Overall, the water bath is only suitable for millimeter-level and non-vitrified samples.

Another convection heat transfer method in practice relies on forced moving hot air as the heating fluid, as shown in Fig. 3C. Hochi *et al.* compared the results of water bath and natural air convection heat transfer with morulae and blastocysts[25]. In this study, the air rewarming rate was less than 250 °C/min, while the water bath warming rate was greater than 1000 °C/min for a 0.25 mL sample. Consequently, slow warming appeared to cause injuries to morulae and blastocysts, as evidenced by the hatching results after cryopreservation. For a 25 mL sample size, Shen demonstrated that air rewarming is not as effective as a water bath in terms of rewarming rate, but it performs better in terms of temperature uniformity[48]. However, air rewarming is not commonly applied to the thawing of cryopreserved samples due to its insufficient rewarming rate.

3 Mechanical Energy Source

3.1 Ultrasound Heating

The ability of ultrasound to safely penetrate deep tissues makes it an attractive option for noninvasive treatment of diseases and internal injuries[64]. Ultrasound heating is converting the mechanical energy of ultrasound waves into heat, governed by the following equation[65]:

$$Q = \alpha \mathrm{I} = \frac{\alpha p^2}{\rho c}$$

Where the Q is the heat generation rate per unit volume (W/m^3), α is the acoustic absorption coefficient of the medium (Np/n/MHz), I is the ultrasound intensity (W/m^2), p is complex pressure profile [Pa], ρ is density of sample[kg/m^3], and c is sound velocity.

By using a focused ultrasonic beam, high-density mechanical energy is delivered to a small region of tissue with little or no effect on the surrounding areas. High-intensity focused ultrasound (HIFU) is widely used in thermal ablation for cancer treatment. HIFU heating using commercial transducers successfully increases the temperature of a tumor sample within a 1 mm diameter at a rate of 1200 °C/min[66]. Olmo *et al.* applied this benefit to the cryopreservation field to elevate cryopreserved samples' temperature from -150 °C[41]. In their study, by varying frequencies and power input, a rewarming rate of 200 °C/min was achieved for organs (~3 cm^3) when applying 75 W and 300 kHz, according to simulation results. Xu *et al.* first demonstrated the rewarming rate experimentally in 2022, achieving a maximum rewarming rate of 57 °C/min (mean 23 °C/min) for 2 mL cryovials, from -20 °C to 5 °C, using 444 kHz ultrasound[42]. Although simulation results showed rapid rewarming rates, experimental confirmation was lacking until 2023. In 2023, Alcalá *et al.* successfully used HIFU to rewarm *Caenorhabditis elegans* nematodes cryopreserved at -80 °C[65]. This method effectively addresses recrystallization challenges by harnessing ultrasound's inherent attenuation properties, reducing the risk of thermal runaway associated with electromagnetic heating, as described in the following section. Unlike electromagnetic rewarming, which is limited by coil positioning, HIFU provides superior flexibility and precision. Building on this progress, Encabo *et al.* achieved the recovery of mouse hearts from cold preservation at -6 °C using the HIFU in 2024[67]. These advancements highlight HIFU's potential as a promising solution for mitigating recrystallization-related issues in rewarming process of cryopreservation.

However, ultrasound propagation is influenced by wavelength, pressure, velocity, power, intensity, sample volume, and material property such as density and acoustic impedance. Thus, HIFU is still limited to small sample sizes due to its low penetration depth, as ultrasound intensity decreases significantly in materials with high acoustic impedance, such as bone[68]. In addition, heating uniformity still needs to be evaluated to better understand the thermal stress during the HIFU heating method. Lastly, HIFU is also limited by ultrasound imaging technology, including challenges like acoustic shadowing, reverberation, and refraction.

Table 1 Water Bath Rewarming Experiments of Cryopreserved Samples

Sample Name	Total Volume (mL)	Water Bath Temperature (°C)	Shaking	Rewarming Rate (°C/min)	Recovery Rate (%)
Rat Islet slice[61]	0.1	37	–	> 1000	79
Bovine embryo[25]	0.25	35	×	> 1000	42.1
Testicular interstitial cell[62]	1	37	√	20	65.3 ± 2.1
Rabbit Carotid Artery[63]	10	37	×	130	71
DPVP Solution[48]	25	37	√	48.2	–

DPVP is a vitrification solution contains 41% (v/v) dimethyl sulfoxide (Sigma Aldrich, St. Louis, MO) and 6% (w/v) polyvinylpyrrolidone (Sigma-Aldrich) in phosphate buffered saline solution (Sigma Aldrich). - means information is not mentioned in cited references.

4 Electromagnetic energy source

4.1 Plasmonic laser heating

Laser heating increases the temperature of cryopreserved samples by absorbing electromagnetic energy in the optical wavelength range. Fig. 4A demonstrates the setup of laser heating and the light scattering effect produced by the nanorods. The laser heating setup consists of near-infrared (NIR) lasers, a collimator, lenses, a magnetic stage, and a sample cuvette, as shown in Fig. 4B. Three beam splitters and four mirrors are included to further enhance heating uniformity. Titanium nitride (TiN) and gold (Au) are the two most commonly used plasmonic nanomaterials dispersed into cryoprotectant agents (CPA) to enhance energy conversion from optical radiation to thermal energy[45]. Daly *et al.* and Khosla *et al.* demonstrated that the pulsed laser (1064 nm) gold nanoparticles (GNs) heating method could raise the temperature of vitrified sample droplets at a rate lager than 1.0×10^7 °C/min for microliter samples[69-70]. In 2021, Zhan *et al.* further proved that the rewarming rate of laser heating for microliter scale samples is 400 times greater than the traditional convective method (water bath)[44]. Compared with GNs, TiN nanoparticles (NPs) are not only less expensive but also exhibit high thermal stability. Meanwhile, TiN NPs demonstrate higher absorption but less scattering than Au nanorods (GNRs), which results in TiN clusters and a higher heating rate compared to Au nanorods. In 2022, Alvarez *et al.* confirmed that TiN NPs improve heat rate, thermal stability, and temperature uniformity compared to GNs[45]. Additionally, a 1μL microdroplet was studied using 1064 nm pulsed laser heating, and devitrification was not observed. Although laser heating achieves a fast-thawing rate, it is still limited to small-size sample due to the laser focus size. Furthermore, the high concentration of GNRs or TiN NPs brings high costs and unknown toxicity.

4.2 Electric energy source

The electric-to-thermal energy conversion heating method integrates principles from both low-frequency conventional electric circuit theory and high-frequency electromagnetic wave theory. The former is based on electric resistance induced by ionic movement known as the Joule effect, whereas the latter utilizes the dielectric effect, which arises from the polarization of dipole molecules such as water and DMSO, as illustrated in Fig. 5. This figure illustrates the oscillation behavior of particles at different frequencies. As frequency increases, smaller masses of matter are preferentially excited due to the relationship among relaxation time, particle mass, and frequency. Dielectric heating leverages this phenomenon by inducing the rotation of dipolar molecules in an alternating electric field, thereby producing volumetric heat through molecular friction.

4.2.1 Joule Heating

Joule heating, a physical effect, is widely applied in medical treatments such as radiofrequency ablation for cancer therapy[71-72]. It occurs when an electric current passes through a resistive conductor, generating heat. Zhan *et al.* were the first to propose a Joule-heating-based platform for rewarming vitrified biosystems[73]. In their system, various biological samples—including adherent cells (~4 μm), *Drosophila melanogaster* embryos (~50 μm), and kidney slices (~1.2 mm)—were placed on an electrical conductor and subjected to pulsed voltage inputs of up to 350 V. By tuning the pulse width, they achieved an ultrafast rewarming rate of 2.4×10^6 °C/min, successfully warming samples from -196 °C to 7.6 °C. Subsequently, Han *et al.* developed a Joule-heating-based electric heating chip that enabled the recovery of 97.2% viability in human lung adenocarcinoma cells and 93.18% in human mesenchymal stem cells (MSCs)[59]. Utilizing approximately 185 W of power (with 4 A

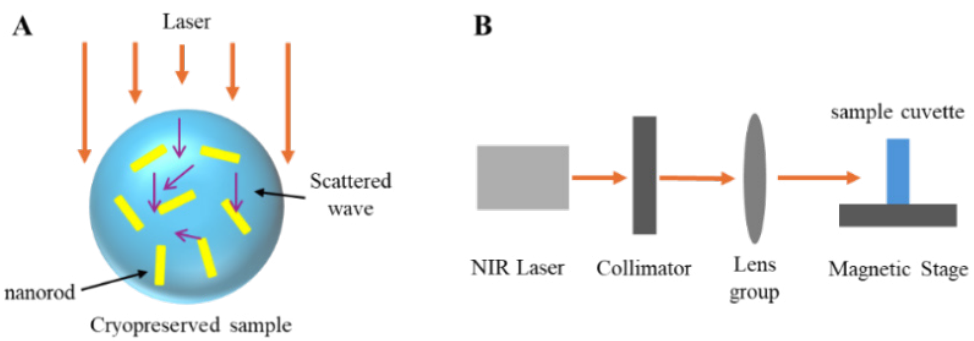

Fig. 4 Heating mechanism of laser rewarming and its setup

(A) The mechanism of laser rewarming with nanorods or nanoparticles infused into the cryopreserved sample. The laser is directed onto the cryopreserved sample, such as cells, and dispersed by the nanorods across the sample volume. The scattered wave uniformly heats the cells. (B) The general setup of the laser rewarming application. NIR, near infrared.

current and 11.6 Ω sheet resistance), they achieved a rewarming rate of 2300 °C/min for a 2.8 mL vitrified solution.

Fig. 6 illustrates two typical configurations of Joule heating structures: a flat sheet (Fig. 6, left) and a sandwich structure conductor (Fig. 6, right). In both designs, heat is generated *via* the intrinsic resistance of the conductor when an electric current is applied and then transferred to the biological sample through conduction. The Joule heating technique offers a straightforward setup and mechanism, akin to that of a conventional resistance heater. However, precise control over key parameters—such as pulse width, voltage magnitude, current amplitude, operation duration, and heat diffusion time—is essential to ensure the rewarming rate exceeds the Critical Warming Rate (CWR) and to avoid overheating, particularly at the interface between the sample and conductors.

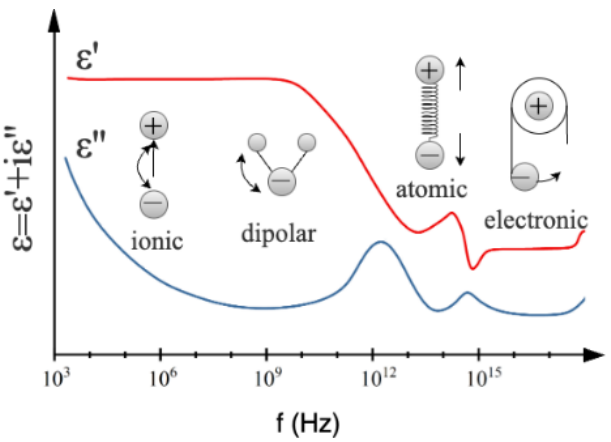

Fig. 5 Relationship between dielectric properties of materials and frequency
As frequency increases, the corresponding wavelength decreases, and the type of oscillating mass shifts from larger entities such as ions to smaller ones such as electrons.

As the size and thickness of biospecimens increase-for instance, in fat tissues or organs-achieving uniform heating becomes increasingly difficult. The contact surface between the sample and the conductor typically reaches the highest temperature, increasing the risk of localized overheating, which can be detrimental to larger or more sensitive samples. Joule heating is governed by the following equation:

$$q' = I^2 R$$

Where *q*' is the heat generation per unit length, I is the current in A, and R is the electric resistance in Ω.

4.2.2 Dielectric Heating

The electromagnetic wave heating effect was first discovered by Percy Spencer in 1945[74]. Subsequently, the conventional microwave was invented in 1947 and became more common in the 1970s[74]. Research into microwave-assisted thawing for cryopreservation applications began in the 1960s[75]. Dipolar molecules, such as water—illustrated in Fig. 7 (left)—possess an internal charge separation due to the high electronegativity of the oxygen atom. Consequently, water molecules tend to align with the direction of an external electric field. Exposed to an alternating electric field, these dipoles continuously reorient, generating substantial heat through molecular friction. This mechanism, known as dielectric heating, is also applicable to other polar compounds commonly used in cryopreservation, such as DMSO and glycerol.

The dielectric heating is governed by the following equation:

$$Q = \omega \cdot \varepsilon''_{eff} \cdot \varepsilon_0 \cdot E^2$$

Where *Q* is the heat generation rate per unit volume, W/m^3, ω is

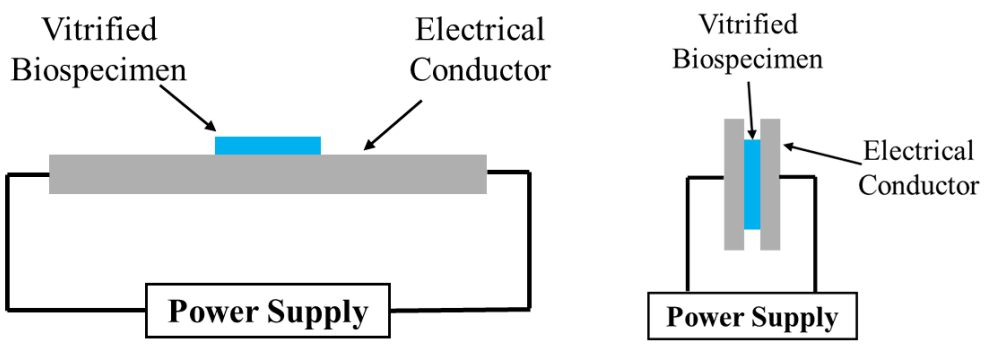

Fig. 6 Schematic diagram of the Joule heating setup
The left panel illustrates a configuration in which the sample is directly placed on a flat sheet electrical conductor. Upon application of power, Joule heating is initiated, with the bottom layer of the sample being heated first due to direct contact with the conductor. The right panel depicts a sandwich structure designed for tissue slices, enabling more uniform heating by enclosing the sample between conductive layers.

the angular frequency of the exciting radiation, rad/s, which equals to 2πf, f is the applied frequency, ε_0 is the permittivity of free space, and E is the electric field strength. ε''_{eff} is the effective relative permittivity loss, which can be classified as dielectric, ε''_d, and conductivity contribution, ε''_σ, expressed by the following equation:

$$\varepsilon''_r = \varepsilon''_d + \varepsilon''_\sigma = \varepsilon''_d + \frac{\sigma}{\omega\varepsilon_0}$$

Where ε''_d is the imaginary part of the complex relative permittivity of the absorbing material, describing the ability to convert electromagnetic field energy into heat; σ is the electric conductivity. For non-conductive material, $\varepsilon''_{eff} = \varepsilon''_d$.

In the following section, currently available dielectric heating applications used in cryopreservation rewarming will be discussed. All of these methods are based on the theoretical principles described above and include: (a) capacitor heating, (b) antenna heating, (c) multi-mode cavity heating, and (d) single-mode resonant cavity heating.

(1) Capacitor heating

Conventional capacitor heating devices typically consist of two electrodes, a coupling coil, a power supply, and a temperature sensor. In 1964, Lehr[76] first introduced the concept of using capacitor heating for organ preservation, proposing several electrode configurations—including concentric cylindrical, parallel plate, and multi-electrode arrangements (Fig. 8)—operating at 27 MHz and 440 W. The concentric cylindrical electrode configuration (Fig. 8A) is suitable only for small samples; for larger specimens, warming rates exceeding 10 °C/min cannot be achieved without significant overheating of tissue adjacent to the internally cooled central electrode. This limitation parallels challenges observed in radiofrequency ablation[72], a minimally invasive technique for cancer treatment. Fig. 8C illustrates a six-electrode heating system designed to deliver heat to three targeted regions of an organ—upper, middle, and lower. However, when attempting thawing rates above 10 °C/min, significant tissue overheating remains unavoidable. This issue arises primarily from the difficulty of accurate temperature monitoring, as thermocouples are unsuitable for use within the electric field, and their placement is technically challenging. Additionally, impedance matching was not addressed in earlier designs.

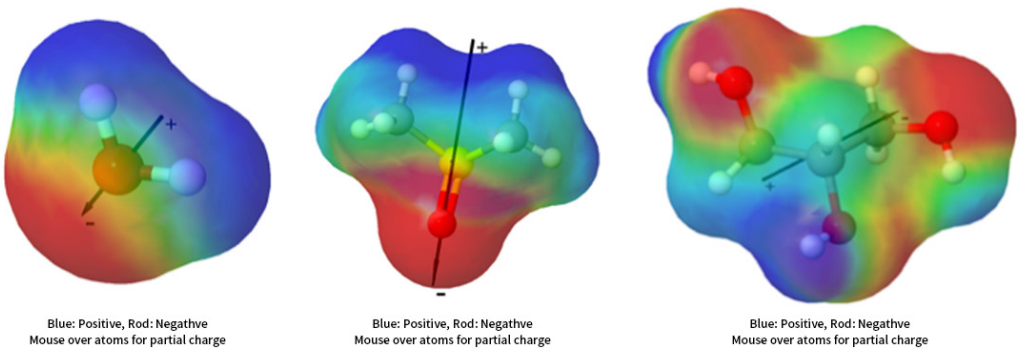

Fig. 7 Molecular structure of water (left), DMSO (middle), and glycerol (right)

The red regions indicate areas of negative charge, while the blue regions represent positive charge. The black arrow denotes the direction of the electric field, illustrating the alignment behavior of dipolar molecules under an applied alternating electric field.

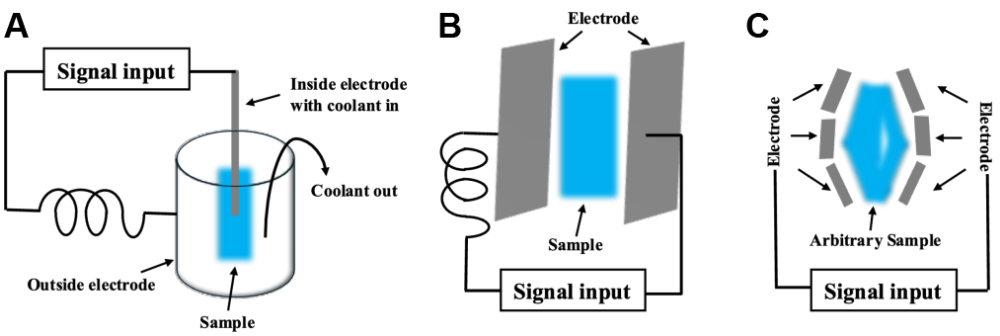

Fig. 8 Configuration of capacitor heating system

(A) Concentric cylindrical electrode configuration; (B) Parallel plate electrode configuration; (C) Multiple electrode configuration. Each setup offers distinct electric field distributions and is suited for different sample sizes and heating uniformity requirements.

More recently, Wowk advanced the development of parallel capacitor heating systems (Fig. 8B) by incorporating impedance matching techniques[77]. In his study, a rabbit kidney perfused with 50 mL of M22 vitrification solution was vitrified and rewarmed at a fixed frequency of 27 MHz with 500 W input power. A peak rewarming rate of approximately 150 °C/min was achieved at -70 °C, with an average rewarming rate of around 55 °C/min between -100 °C and -30 °C. This improved system includes a forward/reverse power meter, parallel and series variable capacitors, dual coupling coils, and a variable attenuator. The forward/reverse power meter monitors the ratio of incident to reflected power, while impedance matching is optimized by adjusting the 0-20 dB variable attenuator to maintain a stable field intensity.

Among the available configurations, the parallel plate capacitor setup is currently the most widely studied. Both Joule heating and parallel capacitor heating employ flat plate electrodes or conductors; however, they differ fundamentally in frequency range and heating mechanism. Unlike Joule heating, capacitor-based dielectric heating induces volumetric heating *via* an alternating electric field, and does not require direct physical contact between the electrodes and the sample.

This configuration offers several advantages: ① deep penetration of the electric field, ② high absorption efficiency of M22 at the designed 27 MHz frequency, and ③ precise control of impedance matching through adjustable capacitors. Nevertheless, several limitations persist:

a. Insufficient rewarming below -100 °C, as noted by Wowk[77];

b. Increased energy loss as electrode spacing grows with sample thickness;

c. Power limitations imposed to prevent voltage breakdown;

d. Safety risks due to the high voltage differential between electrodes;

A low system quality factor (Q), which corresponds to reduced energy efficiency.

(2) Antenna heating

Antenna heating directly heats cryopreserved samples using the incident power from the antenna. While both the electric (E) and magnetic (H) fields are generated by the antenna, biological samples are typically unable to absorb H field energy effectively unless magnetic materials, such as ferrous electro-seeds or magnetic nanoparticles, are added. These additives will be discussed in the section on induction/nanorewarming. Burdette and colleagues[78] designed a horn-shaped antenna system operating at a single frequency (2450 MHz) and a dual frequency system (2450 MHz + 7 MHz) to heat cryopreserved rabbit (*N* = 74) and canine (*N* = 27) kidneys. The 7 MHz antenna is placed orthogonal to the 2450 MHz source to enhance the uniformity for larger samples, such as canine kidneys, by taking advantage of the larger penetration depth and specific local doping ferrous electro-seed. Later, 918 MHz was applied by the same group but achieved better temperature uniformity for 27 canine kidneys without the need for additives. Unfortunately, no vitrification or transplantation studies were performed. Recently, a hybrid warming method combining traditional convective heating[79] *via* a water bath with a helical antenna has been explored for use with 1.8 mL cryovials (Fig. 9, right). This system incorporates signal input from the coaxial feeder, and the helical antenna excites an axial E-field while the water bath provides supplemental heat. Although this approach achieved a high rewarming rate of 100.05 °C/min with 3 W input power, the sample size remained limited to less than 1.8 mL due to the space occupied by the helical antenna.

Both horn and helical antenna heating systems offer distinct advantages. Horn antenna heating[80] can handle larger power inputs without risking damage to the antenna, unlike helical antennas, which may sustain damage from reflected power when the input power is significantly increased. Additionally, horn antennas are suitable for heating cell suspensions, tissues, and various organ types. Conversely, inserting helical or other uniquely shaped antennas directly into organs can be challenging without compromising the structural integrity of the samples. Nevertheless, a hybrid heating approach combining helical antennas with a water bath provides a cost-effective and sufficient method for heating cell suspensions, with potential for scaling up sample sizes.

(3) Multimode cavity heating

Ketterer *et al.*, Guttman *et al.*, Rachman *et al.*[80], and Pegg *et al.* have successively reported the use of microwave thawing for canine kidneys at a frequency of 2.45 GHz[75,80-82]. However, the limited penetration depth associated with high frequencies results in non-uniform heating across the radius of biological samples. Furthermore, the uneven distribution of the electric field can lead to 'thermal runaway,' a phenomenon that worsens as the material's ability to absorb electrical field energy increases with rising temperature. To address this issue, the multi-mode cavity was designed to improve the uniformity of the electrical wave peaks within the chamber. However, real-time analysis and control of the multi-mode cavity system are challenging due to the complex permittivity of the material, which varies with temperature and frequency[83]. As the temperature increases, changes in the real part of the permittivity of cryopreserved samples lead to off-resonance and shifts in the peak electric field, which constrain further development and application of this technology.

(4) Single-mode resonant cavity heating

Due to the challenges associated with multi-mode cavities or commercial microwave ovens, a single-mode resonant cavity appears more promising for providing not only high intensity and uniform electric fields but also greater predictability and control[84]. Two common configurations of single-mode resonant cavities are cylindrical and rectangular. Given the potential future application to organs, a rectangular cavity (shown in Fig. 10A) was developed by Luo[46] in 2006, operating at 434 MHz, to ensure adequate size allowance, penetration depth, and ease of manufacturing. This is because a cylindrical cavity is smaller than a rectangular one at the same frequency.

To excite a single standing wave inside the cavity (single mode), the concept of the dominant mode is crucial. Every cavity has a cut-off frequency and resonant frequencies for different modes. When the input frequency is below the cut-off frequency (the first mode), no mode will be excited in the cavity. Conversely, when the frequency is above the secondary mode frequency, two or more modes may exist within the cavity. Therefore, the desired frequency of 434 MHz must be greater than the cut-off frequency but lower than the secondary mode frequency for the designed cavity. The governing equations for the cut-off frequency and resonant frequency are as follows, assuming air-filled media inside the cavity:

$$f_c = \frac{1}{2\sqrt{\varepsilon\mu}}\sqrt{(\frac{m}{a})^2 + (\frac{n}{b})^2}$$

$$f_{nmp} = \frac{c}{2}\sqrt{\left(\frac{m}{a}\right)^2 + \left(\frac{n}{b}\right)^2 + \left(\frac{p}{d}\right)^2}$$

Where f_c is the cutoff frequency of the waveguide, and are the material permittivity and permeability, m, n, p is the mode number, determining the number of half wavelength in x, y, and z directions shown in Fig. 11B, f_{nmp} is the cavity resonant frequency, and c is the speed of light.

In Luo's study, the cavity (0.40m × 0.35m × 0.68m) was intentionally designed to correspond to a 434 MHz frequency to generate a single standing wave. The study proposed the heating results of cryopreserved samples (36 mm diameter) from -80 °C within the single-mode resonant cavity, operating in TE 101 mode[46]. The governing equations ffor the electric and magnetic fields in the TE101 mode cavity are as follows, with E_z, E_x and H all equaling zero:

$$H_z = -j2AC\,cos(k_x x)sin(k_z x)$$

$$H_x = \frac{j2ACk_z k_x\, sin(k_x x)cos\,(k_z z)}{k^2 - k_z^2}$$

$$E_y = \frac{-2AC\omega\mu\, k_x sin(k_x x)sin(k_z z)}{k^2 - k_z^2}$$

The system comprises three subsystems: the microwave subsystem, the thermal subsystem, and the cavity and cooling subsystem. The microwave subsystem includes a frequency synthesizer, power amplifier, directional coupler, power meter, personal computer control, and a dummy load. The thermal subsystem monitors the sample temperature in real-time. Pan *et al.* further developed the SMER heating system to investigate the dielectric properties of cryoprotectants (CPAs)[85] and conducted numerical simulations on[47]. Fig. 10D and 10E show the electric and magnetic field simulations of the SMER system using COMSOL, demonstrating the high intensity and uniformity

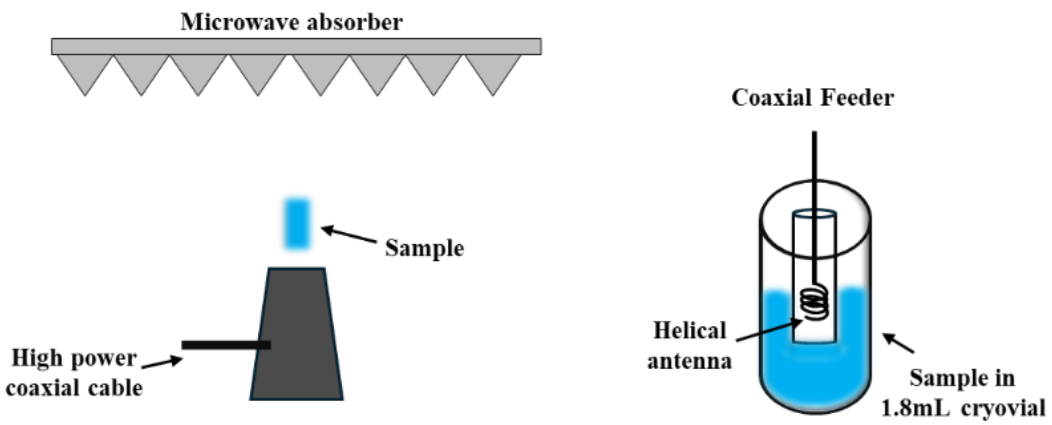

Fig. 9 Schematic drawing of the antenna heating systems

The left panel illustrates a horn antenna system equipped with a microwave absorber. The microwave absorber is employed to prevent reflected waves from disrupting the electric field, and should be integrated within the horn antenna. The right panel depicts the hybrid helical antenna heating method combined with a water bath. The water bath is placed outside the sample holder to enhance heating efficiency.

of the electric field at the center of the cavity under the TE101 mode. The effect of sample shape was also explored[47,86].

In addition, an investigation was conducted on a distinct inverted U-shaped dielectric loss observed in specific CPAs, such as DPVP and EPVP. This characteristic helps mitigate thermal runaway by reducing the rate at which electromagnetic energy is converted into thermal energy above -40 °C, based on molecular dynamics principles[87-88]. As a result, the rewarming rate in high-temperature area is lower than that of low-temperature areas, ensuring improved temperature uniformity. In 2021, Ren *et al.* prototyped an auto-loading system integrated with the SMER system (shown in Fig. 10C) and reported the comparison between natural air, water bath, and SMER with a 400W power supply in a 25 mL CPA solution. The SMER system achieved a rewarming rate of 331.63 ± 8.59 °C/min while

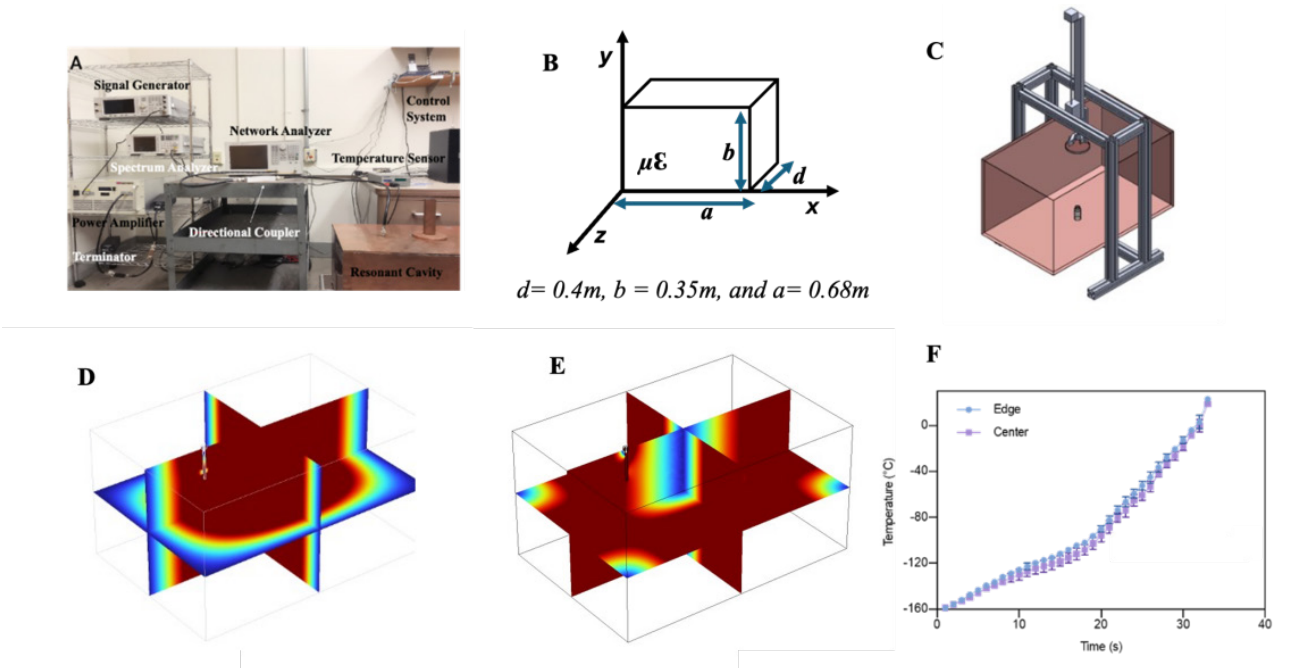

Fig. 10 SMER technology setup and results

(A)-(C) A schematic diagram of the SMER cavity with automatic loading and unloading system. (D) & (E) The simulation of the electric and magnetic field distribution. (F) The rewarming rate of the 25 mL DPVP solution from vitrified state to room temperature.

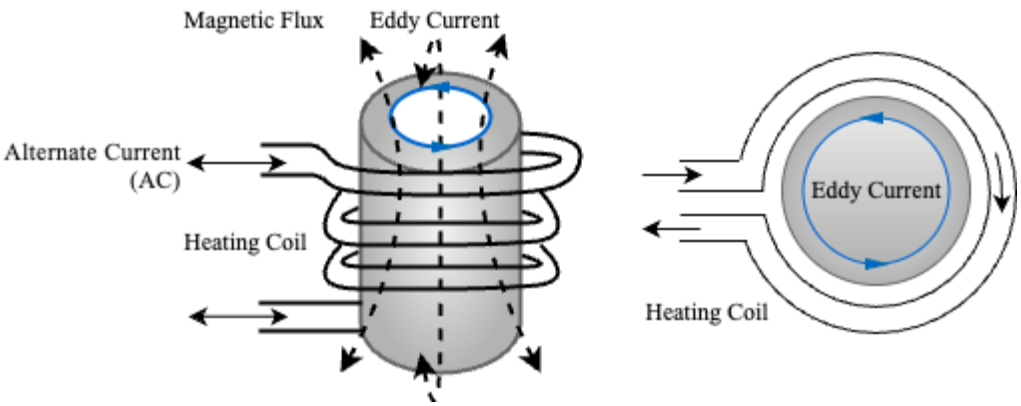

Fig. 11 Eddy current illustration

The left figure shows a 3D representation of the eddy current generated by an alternating current-induced magnetic field. As the direction of the current changes, a magnetic flux is created and is located at the center of the coil. The right figure displays the top cross-section view. Eddy currents occur when the magnetic field is tangential to the surface of the conductive material.

limiting the maximum thermal gradient to less than 1 °C/mm, as shown in Fig. 12F[48]. Currently, SMER is being applied to rabbit jugular veins[89] and is effective for larger size tissues and organ samples.

Although the SMER system is promising for a 25 mL sample, future development is needed to enhance resonant tracking by adjusting the incident frequency. This adjustment method differs from the capacitor tuning described in the capacitor heating section, where the SMER system adjusts the frequency to tune the system's load impedance and achieve resonant/impedance matching. This approach has the potential for extreme-seeking control and noise reduction[90].

Overall, significant attention has been given to electric heating due to its high-power intensity capability across both low and high frequencies. Various applications have been developed, each with its own advantages and limitations. However, common requirements and challenges for electric heating include the need to control the power feed bandwidth, frequency, sample size, and impedance/resonant tuning to maintain a constant high rewarming rate.

4.3 Magnetic energy source

Similar to electric field heating, magnetic heating also enables volumetric heating of the reactive material, a process known as induction heating. Induction heating relies on the eddy current or hysteresis effect. Regardless of the specific mechanism used in magnetic heating, a thermal seed is required for cryopreservation, such as nanoparticles, metal mesh, metal foil, or metal foam. There are additional effects associated with magnetic heating mechanisms, such as Néel Relaxation and Brownian Relaxation, though these have not yet been applied to cryopreservation.

(1) Eddy current effect

Eddy current are generated when a tangential magnetic field interacts with the surface of a conductive material. This results in the production of eddy currents on the conductive surface, which in turn causes Joule heating. Fig. 11 illustrates the eddy current beneath a heating coil, governed by the equation below:

$$W_{diss} = \frac{R_s}{2}\int_{wall}|H_{tan}|^2 ds$$

Manuchehrabadi[52] studied Eddy current-induced rewarming for cell suspension using copper foam, aluminum foil, and nitinol mesh, achieving 1200 °C/min in 1.8mL vitrified samples in cryovial with RF power of 1kW. This study found that to successfully convert magnetic field energy to eddy current, the foil thickness needs to be 4 times the penetration depth of the aluminum foil, depending on the surface properties and applied frequency.

(2) Hysteresis effect/nano-rewarming

The hysteresis effect encompasses various types, with magnetic hysteresis being one of the most prominent. This effect depends on the stored and released magnetic field energy (H) within magnetic materials, such as magnetic nanoparticles, which are commonly used in nano-rewarming technology. When a positive magnetizing force is applied, the magnetic material progresses from 0 to A (as shown by the dashed line). Once the field is removed or reversed, the material follows the path from A to B to C to D, as depicted in Fig. 12. When the magnetic field direction is switched again, the curve follows from D to E to F to A.

The hysteresis loss effect occurs when a magnetic material is subjected to an alternating magnetic field, causing the magnetic dipoles to oscillate and reverse polarity with each cycle. This oscillation leads to considerable internal friction, generating heating within the material[91]. The enclosed area i in the hysteresis loop represents the energy loss due to the

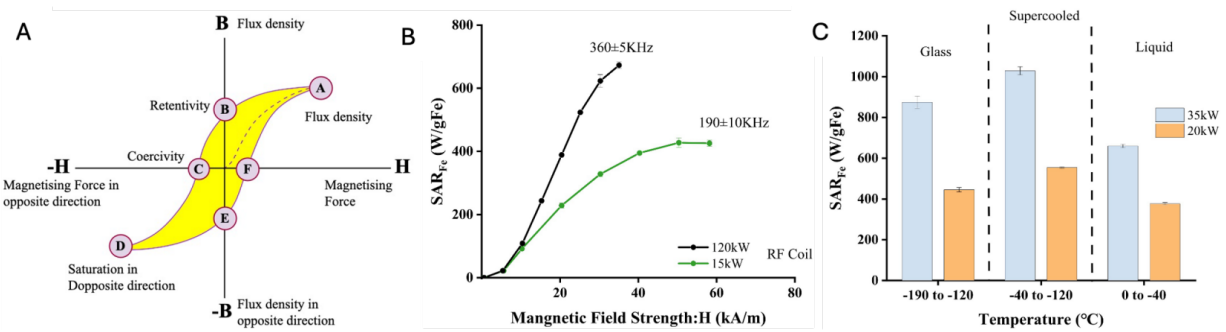

Fig. 12 Magnetic hysteresis effect and nanowarming results

(A) Illustration of the magnetic hysteresis curve (B-H). (B) Relationship between magnetic field strength and the specific absorption rate (SAR) at frequencies of 360 and 190 kHz, with power levels of 120 kW and 15 kW, respectively. SAR represents the rate at which energy is absorbed by biological tissue exposed to an electromagnetic field. (C) SAR of magnetic nanoparticles at various temperatures and magnetic field strengths.

magnetic hysteresis effect, as shown in Fig. 12A. The average heat generation, q, is expressed as:

$$q = P_v = k \cdot f^a \cdot B^b$$

Where P_v is the time-averaged power loss per unit volume (mW/cm^3), f is the frequency in kHz, and B is the peak magnetic flux density. The constants k, a and b are the Steinmetz coefficients, which are material parameters typically determined empirically through fitting the materials B-H hysteresis curve.

Based on the magnetic hysteresis effect, a research group at the University of Minnesota initiated the radiofrequency (RF) nanowarming technology, which depends on the excitation of magnetic nanoparticles (SNPs) by the magnetic field. Etheridge *et al.* first presented proof of concept RF nanowarming to achieve 200 °C/min for 1 mL CPA solution containing 10 mg Fe/ml samples when supplying 1kW power[51]. Building on this study, Manuchehrabadi *et al.* scaled up the RF nanowarming system to an 80 mL physical system[52]. were successfully thawed and transplanted by the same group in 2023[53]. Long-term vitrified rat kidneys were successfully thawed and transplanted by the same group in 2023[92], and they are currently exploring vitrification and nanowarming for human-sized organs[93]. In addition, they are actively working on the nanoparticles development[94-95] and CPAs loading protocol[96]. Nanowarming, which harnesses nanomaterials and the magnetic hysteresis effect, appears to be a promising method for scaling up cryopreservation while ensuring rapid and uniform heating.

5 Comparison and discussion

In summary, traditional water baths cannot ensure rapid and uniform rewarming to prevent lethal ice recrystallization and thermal stress in large samples, such as tissues and organs. Laser and ultrasound heating are also limited to small-scale samples. As a result, dielectric and induction heating mechanisms become more attractive due to their ability to provide large-scale volumetric heating. Each of these methods has its own advantages, limitations, and potential for improvement, which are discussed below.

(1) Power usage: Dielectric heating consumes significantly less power than induction heating methods, which rely on eddy current and hysteresis effects[50]. Recent research demonstrates this efficiency gap, with nanowarming requiring a 120 kW power source, while comparable dielectric heating needs only 500 W. This discrepancy underscores the poor energy conversion between magnetic field energy and thermal energy. Such inefficiency creates an additional challenge: RF nanowarming systems require extensive cooling infrastructure to prevent coil overheating. On the other hand, dielectric heating, despite its energy efficiency, faces its own limitations. The dielectric signal generators and power amplifiers are costlier than induction coil systems, which are already well-established in industrial applications. This cost disparity ultimately constrains the scalability of dielectric heating technologies.

(2) Additives: Dielectric heating takes advantage of the dipolar nature of water/CPAs, meaning nanoparticles are not required, as the water and CPAs serve as the energy absorption medium. In contrast, nanoparticles or seeds are necessary for nanowarming. Additionally, biocompatibility must be considered for additives in both methods.

(3) Control theory: Dielectric heating requires sophisticated control to meet impedance-matching requirements throughout the thawing process. SMER (single-mode electromagnetic radiation) heating offers significant advantages in field prediction and control due to the presence of only one mode. In contrast, induction heating does not face this limitation, as it operates as an open system.

(4) Thermal runaway: Both dielectric and induction heating methods must carefully manage the issue of thermal runaway. This challenge arises from the dependence of thermal runaway on material properties, making it a critical concern for both heating techniques.

(5) Hysteresis effect: Fig. 12B and 12C illustrate the specific absorption rate (SAR) of nanoparticles in various frequencies and magnetic field strengths. The slope of SAR decreases as the magnetic field increases for both 360 kHz (red) and 190 kHz (blue). A higher frequency significantly increases the SAR when the same magnetic field is applied, likely due to changes in relative permeability with frequency. The magnetic hysteresis effect shows promise for improving rewarming performance at low temperatures (below -100 °C). This observation aligns with the hysteresis effect diagram in Fig. 12A, where a higher magnetic field strength results in only a small increase near the boundary area, indicating lower efficiency. In addition, a maximum SAR is observed in the system, marked by a red line around 50 kA/m, likely indicating the saturation point of the magnetic nanoparticles. Dielectric heating using 27MHz lacks the ability to rewarm samples below -100 °C[77]. For dielectric heating, the hysteresis effect is observed in ferroelectric materials, a type of dielectric material, which might enhancing rewarming performance. However, solubility issues arise, as most ferroelectric materials do not dissolve in water.

(6) Cost-effective: Both SMER and nanowarming technologies utilize radiofrequency electromagnetic waves, but with

distinct implementations. SMER operates at significantly higher frequencies in the MHz range, which increases equipment costs. Conversely, nanowarming works at lower frequencies but requires high-power amplifiers and substantial cooling systems, which also elevate equipment expenses. This makes direct comparison of capital equipment costs difficult. However, operational and maintenance costs in clinical applications are likely to be lower for SMER technology due to its lower power usage.

(7) Clinical operability: Since cryopreservation rewarming devices are ultimately intended for use by medical staff with limited technical or engineering backgrounds, clinical implementation requires a user-friendly design. Both technologies should feature single-button operation and automatic shutdown capabilities to ensure ease of use. A key distinction between the two methods lies in their physical setups: SMER utilizes a contained cavity system, while nanowarming employs an open RF coil that requires dedicated space similar to MRI facilities. Additionally, nanowarming's substantial power requirements may necessitate new infrastructure within hospitals, potentially complicating installation and increasing implementation costs.

6 Conclusion

Rewarming mechanisms and their applications in cryopreservation have been extensively studied, focusing on three primary energy sources: thermal, mechanical, and electromagnetic. Traditional thermal energy sources, such as hot plates and water baths, have been widely used. HIFU is a notable application of mechanical energy, offering volumetric heating, but it is currently limited by small sample sizes and energy intensity. Among electromagnetic methods, dielectric heating and induction heating are the most promising. Dielectric heating operates on the principle of dipolar molecular rotation, whereas induction heating relies on the eddy current effect and magnetic hysteresis. However, since eddy currents are surface effects that do not provide volumetric heating, magnetic hysteresis becomes the dominant heating mechanism in applications like nanowarming. Currently, nanowarming has shown significant progress in rewarming small animal organs and in theoretical models for human organs. Meanwhile, dielectric heating also presents substantial potential for cryopreservation of large samples, particularly in systems like SMER.

Future advancements in cryopreservation rewarming technology will continue to focus on achieving rapid, uniform volumetric heating of large biological samples. This will require parallel development across multiple fronts, including optimizing CPAs to reduce toxicity while enhancing vitrification properties, engineering biocompatible nanoparticles with improved electromagnetic responsiveness, and deepening our understanding of electromagnetic field interactions within vitrified tissues. Additionally, addressing scalability challenges for larger specimens will be critical. Potential breakthrough areas include the development of universal biocompatible nanoparticles, AI-driven parameter optimization, hybrid systems combining the advantages of SMER and nanowarming approaches, and user-friendly designs suitable for clinical implementation with minimal infrastructure requirements. Success in these areas could revolutionize organ preservation, significantly expanding transplantation windows and improving patient outcomes.

Acknowledgments

Not applicable.

Research ethics

Not applicable.

Informed consent

Not applicable.

Author contributions

Ma R D: Constructing an idea for this review article and write the manuscript, draw figures drawing, revising and conduct the literature review; Wang Z Y: Revise the article, Literature review; Ren S, Gao D Y: Critical review and revise; Shu Z Q, Chen M, Gao D Y: Organizing and supervising the review.

Use of large language models, AI and machine learning tools

No LLM, AI or machine learning tool was used for any part of the present study.

Research funding

This study was supported by National Natural Science Foundation of China (Award Number: 2346842).

Conflict of interest

The authors declare that they have no known competing financial interests or personal relationships that could have appeared to influence the work reported in this paper.

Data availability

Due to it is a review paper, supporting data is included in the cited articles.

References

[1] Polge C, Smith A U, Parkes A S. Revival of spermatozoa after vitrification and dehydration at low temperatures. Nature, 1949; 164(4172): 666.

[2] Yánez-Ortiz I, Catalán J, Rodríguez-Gil J E, *et al.* Advances in sperm cryopreservation in farm animals: Cattle, horse, pig and sheep. Anim Reprod Sci, 2022, 246: 106904

[3] Bedaiwy M A, El-Nashar S A, El Saman A M, *et al.* Reproductive outcome after transplantation of ovarian tissue: a systematic review. Hum Reprod, 2008; 23(12): 2709-2717.

[4] Comizzoli P. Biobanking efforts and new advances in male fertility preservation for rare and endangered species. Asian J Androl, 2015; 17(4): 640-645.

[5] Sharafi M, Borghei-Rad S M, Hezavehei M, *et al.* Cryopreservation of semen in domestic animals: a review of current challenges, applications, and prospective strategies. Animals-Basel, 2022; 12(23): 3271.

[6] Pence V C, Bruns E B. The tip of the iceberg: cryopreservation needs for meeting the challenge of exceptional plant conservation. Plants-Basel, 2022; 11(12): 1528.

[7] Rudick B, Opper N, Paulson R, *et al.* The status of oocyte cryopreservation in the united states. Fertil Steril, 2010; 94(7): 2642-2646.

[8] Kim S S, Battaglia D E, Soules M R. The future of human ovarian cryopreservation and transplantation: fertility and beyond. Fertil Steril, 2001; 75(6): 1049-1056.

[9] Pomeroy K O, Comizzoli P, Rushing J S, *et al.* The art of cryopreservation and its changing landscape. Fertil Steril, 2022; 117(3): 469-476.

[10] Wowk B. Thermodynamic aspects of vitrification. Cryobiology, 2010; 60(1): 11-22.

[11] Huang Y, Dong Y, Gao B, *et al.* Transmembrane water transport and intracellular ice formation of human umbilical vein endothelial cells during freezing. Biopreserv Biobank, 2022; 20(4): 311-316.

[12] Ma R, Peng J, Ren S, *et al.* Development of a 3-in-1 multifunctional cell processing system and optimization of cell type-dependent protocols for CPA addition/removal. Int Commun Heat Mass Transfer, 2025; 161: 108511.

[13] Hoffman D I, Zellman G L, Fair C C, *et al.* Cryopreserved embryos in the united states and their availability for research. Fertil Steril, 2003; 79(5): 1063-1069.

[14] Massip A, Vanderzwalmen P, Ectors F. Recent progress in cryopreservation of cattle embryos. Theriogenology, 1987; 27(1): 69-79.

[15] Gao F, Ma R, Ren S, *et al.* Cryopreservation and biobanking of gametes, embryos, and reproductive tissues. Biopreserv Biobank, 2024; 22(1): 1-3.

[16] Taylor M J, Weegman B P, Baicu S C, *et al.* New approaches to cryopreservation of cells, tissues, and organs. Transfus Med Hemother, 2019; 46(3): 197-215.

[17] Ruiz-Delgado G J, Mancias-Guerra C, Tamez-Gomez E L, *et al.* Dimethyl sulfoxide-induced toxicity in cord blood stem cell transplantation: report of three cases and review of the literature. Acta Haematol, 2009; 122(1): 1-5.

[18] Triana E, Ortega S, Azqueta C, *et al.* Thawing of cryopreserved hematopoietic progenitor cells from apheresis with a new dry-warming device. Transfusion, 2013; 53(1): 85-90.

[19] Shu Z Q, Hughes S M, Fang C F, *et al.* A study of the osmotic characteristics, water permeability, and cryoprotectant permeability of human vaginal immune cells. Cryobiology, 2016; 72(2): 93-99.

[20] Wang L, Fu R, Xu C, *et al.* Methods and applications of full-field optical coherence tomography: a review. J Biomed Opt, 2022; 27(5): 050901.

[21] Mazur P, Leibo S P, Chu E H. A two-factor hypothesis of freezing injury. Evidence from chinese hamster tissue-culture cells. Exp Cell Res, 1972; 71(2): 345-355.

[22] Gao D, Critser J K. Mechanisms of cryoinjury in living cells. ILAR J, 2000; 41(4): 187-196.

[23] Mazur P. Freezing of living cells: mechanisms and implications. Am J Physiol, 1984; 247(3 Pt 1): C125-142.

[24] Karlsson J O M, Toner M. Long-term storage of tissues by cryopreservation: critical issues. Biomaterials, 1996; 17(3): 243-256.

[25] Hocki S, Semple E, Leibo S P. Effect of cooling and warming rates during cryopreservation on survival of *in vitro*-produced bovine embryos. Theriogenology, 1996; 46(5): 837-847.

[26] Bank H. Visualization of freezing damage. 2. Structural alterations during warming. Cryobiology, 1973; 10(2): 157-170.

[27] Fahy G M M D R, Angell C A, *et al.* Vitrification as an approach to cryopreservation. Cryobiology, 1984; 21(4): 407-426.

[28] Amorim C A, Curaba M, Van Langendonckt A, *et al.* Vitrification as an alternative means of cryopreserving ovarian tissue. Reprod Biomed Online, 2011; 23(2): 160-186.

[29] Shi Q, Xie Y, Wang Y, *et al.* Vitrification versus slow freezing for human ovarian tissue cryopreservation: a systematic review and meta-analysis. Sci Rep, 2017; 7(1): 8538.

[30] Sharma A, Lee C Y, Namsrai B E, *et al.* Cryopreservation of whole rat livers by vitrification and nanowarming. Ann Biomed Eng, 2023; 51(3): 566-577.

[31] Solanki P K, Rabin Y. Thermomechanical stress analysis of rabbit kidney and human kidney during cryopreservation by vitrification with the application of radiofrequency heating. Cryobiology, 2021; 100: 180-192.

[32] Zhao G, Liu Z F, Zhang A L, *et al.* Theoretical analyses of thermal stress of blood vessel during cryopreservation. Cryo Letters, 2005; 26(4): 239-250.

[33] Solanki P K, Bischof J C, Rabin Y. Thermo-mechanical stress analysis of cryopreservation in cryobags and the potential benefit of nanowarming. Cryobiology, 2017; 76: 129-139.

[34] Hua Z Z, Xu H Y, Zhou G Y, *et al.* Analyses of thermal stress and fracture during cryopreservation of blood vessel. Sci China Ser E-Technol Sci, 2000; 44: 158-163.

[35] Peng J, Ma R, Ren S, *et al.* A study of thermal stress generation during the rewarming process of cryopreserved large biomaterials. Cryobiology, 2021; 103: 167-168.

[36] Yong K W, Laouar L, Elliott J A W, *et al.* Review of non-permeating cryoprotectants as supplements for vitrification of mammalian tissues. Cryobiology, 2020; 96: 1-11.

[37] Bunnik E M. Ethics of allocation of donor organs. Curr Opin Organ Tran, 2023; 28(3): 192-196.

[38] Panda K, Mazumder A, Krishnamurthy A. Kidneychain: leveraging blockchain & artificial intelligence for a streamlined organ donation solution. medRxiv, 2024.

[39] Baust J G, Gao D, Baust J M. Cryopreservation: an emerging paradigm change. Organogenesis, 2009; 5(3): 90-96.
[40] Giwa S, Lewis J K, Alvarez L, *et al.* The promise of organ and tissue preservation to transform medicine. Nat Biotechnol, 2017; 35(6): 530-542.
[41] Olmo A, Barroso P, Barroso F, *et al.* The use of high-intensity focused ultrasound for the rewarming of cryopreserved biological material. IEEE Trans Ultrason Ferroelectr Freq Control, 2021; 68(3): 599-607.
[42] Xu R, Bradley E T, Eleanor M. Experiments and simulations demonstrating the rapid ultrasonic rewarming of frozen beef cryovials. arXiv preprint arXiv, 2022; 153(1): 517.
[43] Liu Y, Kangas J, Wang Y, *et al.* Photothermal conversion of gold nanoparticles for uniform pulsed laser warming of vitrified biomaterials. Nanoscale, 2020; 12(23): 12346-12356.
[44] Zhan L, Guo S Z, Kangas J, *et al.* Conduction cooling and plasmonic heating dramatically increase droplet vitrification volumes for cell cryopreservation. Adv Sci(Weinh), 2021; 8(11): 2004605.
[45] Alvarez C, Berrospe-Rodriguez C, Wu C, *et al.* Photothermal heating of titanium nitride nanomaterials for fast and uniform laser warming of cryopreserved biomaterials. Front Bioeng Biotechnol, 2022; 10: 957481.
[46] Luo D, Yu C, He L, *et al.* Development of a single mode electromagnetic resonant cavity for rewarming of cryopreserved biomaterials. Cryobiology, 2006; 53(2): 288-293.
[47] Pan J, Ren S, Sekar P K, *et al.* Investigation of electromagnetic resonance rewarming enhanced by magnetic nanoparticles for cryopreservation. Langmuir, 2019; 35(23): 7560-7570.
[48] Ren S, Shu Z, Pan J, *et al.* Single-mode electromagnetic resonance rewarming for the cryopreservation of samples with large volumes: a numerical and experimental study. Biopreserv Biobank, 2022; 20(4): 317-322.
[49] Wang Z, Shu Z, Ren S, *et al.* Development of electromagnetic warming technology for cryopreservation. Annual Review of Heat Transfer, 2024; 27: 319-356.
[50] Wang Z, Ren S, Shu Z, *et al.* An efficient and effective electromagnetic rewarming platform for cryopreservation. Cryobiology, 2024; 117: 104987.
[51] Etheridge M L, Xu Y, Rott L, *et al.* RF heating of magnetic nanoparticles improves the thawing of cryopreserved biomaterials. Technology, 2014; 2(3): 229-242.
[52] Manuchehrabi N, Gao Z, Zhang J, *et al.* Improved tissue cryopreservation using inductive heating of magnetic nanoparticles. Sci Transl Med, 2017; 9(379): 4586.
[53] Sharma A, Rao J S, Han Z, *et al.* Vitrification and nanowarming of kidneys. Adv Sci(Weinh), 2021; 8(19): e2101691.
[54] Rollig C, Babatz J, Wagner I, *et al.* Thawing of cryopreserved mobilized peripheral blood: comparison between waterbath and dry warming device. Cytotherapy, 2002; 4(6): 551-555.
[55] Kilbride P, Meneghel J, Creasey G, *et al.* Automated dry thawing of cryopreserved haematopoietic cells is not adversely influenced by cryostorage time, patient age or gender. Plos One, 2020; 15(10): e0240310.
[56] Petrenko V, Whitworth R. Thermal properties of ice. Physics of ice. Oxford: Oxford University Press, 1999.
[57] Marquet P. On the computation of moist-air specific thermal enthalpy. Q J Roy Meteor Soc, 2015; 141(686): 67-84.
[58] Melinder A. Thermophysical properties of aqueous solutions used as secondary working fluids. Stockholm: Royal Institute of Technology KTH, 2007.
[59] Han H X, Zhan T J, Cui M D, *et al.* Investigation of rapid rewarming chips for cryopreservation by Joule heating. Langmuir, 2023; 39(31): 11048-11062.
[60] Pegg D E. The history and principles of cryopreservation. Seminars in Reproductive Medicine, 2002; 20(3): 247-256.
[61] Bank H L, Davis R F, Emerson D. Cryogenic preservation of isolated rat islets of langerhans - effect of cooling and warming rates. Diabetologia, 1979; 16(3): 195-199.
[62] Gurina T M, Pakhomov A V, Polyakova A L, *et al.* The development of the cell cryopreservation protocol with controlled rate thawing. Cell Tissue Bank, 2016; 17(2): 303-316.
[63] Song Y C, Pegg D E, Hunt C J. Cryopreservation of the common carotid artery of the rabbit: optimization of dimethyl sulfoxide concentration and cooling rate. Cryobiology, 2020; 93: 18-26.
[64] Siu J Y, Liu C, Zhou Y. High-intensity focused ultrasound ablation around the tubing. PLoS One, 2017; 12(11): e0188206.
[65] Prakash P, Salgaonkar V A, Diederich C J. Modelling of endoluminal and interstitial ultrasound hyperthermia and thermal ablation: applications for device design, feedback control and treatment planning. Int J Hyperther, 2013; 29(4): 296-307.
[66] Zhou Y F. High intensity focused ultrasound in clinical tumor ablation. World J Clin Oncol, 2011; 2(1): 8-27.
[67] Encabo L, Alcala E, Lopez-Soria J, *et al.* Hifu rewarming of organs after cold preservation: ex vivo assessment of heart performance in murine model. Transplantation, 2024; 108(1): E15-E7.
[68] Ziskin M C. Fundamental physics of ultrasound and its propagation in tissue. Radiographics, 1993; 13(3): 705-709.
[69] Daly J, Zuchowicz N, Nunez Lendo C I, *et al.* Successful cryopreservation of coral larvae using vitrification and laser warming. Sci Rep, 2018; 8(1): 15714.
[70] Khosla K, Zhan L, Bhati A, *et al.* Characterization of laser gold nanowarming: a platform for millimeter-scale cryopreservation. Langmuir, 2019; 35(23): 7364-7375.
[71] Habibi M, Berger R D, Calkins H. Radiofrequency ablation: technological trends, challenges, and opportunities. EP Europace, 2021; 23(4): 511-519.
[72] Zheng H, Li P C, Ma R D, *et al.* Development of a three-dimensional multi-modal perfusion-thermal electrode system for complete tumor eradication. Cancers, 2022; 14(19): 4768.
[73] Zhan L, Han Z H, Shao Q, *et al.* Rapid joule heating improves vitrification based cryopreservation. Nat Commun, 2022; 13(1): 6017.
[74] Osepchuk J M. The history of the microwave oven: a critical review. IEEE, 2009.
[75] Pegg D E, Green C J, Walter C A. Attempted canine renal cryopreservation using dimethyl sulphoxide helium perfusion and microwave thawing. Cryobiology, 1978; 15(6): 618-626.
[76] Lehr H B, Berggren R B, Summers A L, *et al.* Freezing and thawing of large organs. Cryobiology, 1964; 1(2): 194-197.
[77] Wowk B, Phan J, Pagotan R, *et al.* 27 mhz constant field dielectric warming of kidneys cryopreserved by vitrification. Cryobiology, 2024; 115: 104893.
[78] Burdette E C, Karow A M, Jeske A H. Design, development, and performance of an electromagnetic illumination system for thawing cryopreserved kidneys of rabbits and dogs. Cryobiology, 1978; 15(2): 152-167.
[79] Ruan H L, Wang T, Gao C. Microwave-water bath hybrid warming for frozen cryoprotectant solution using a helical antenna. Cryoletters, 2020; 41(1): 26-30.

[80] Rachman M J, Evans S, Pegg D E. Experimental results on the rewarming of a cryopreserved organ phantom in a uhf field. J Biomed Eng, 1992; 14(5): 397-403.
[81] Ketterer F D, Holst H I, Lehr H B. Improved viability of kidneys with microwave thawing. Proc Cryobiol, 1971; 8(3): 309-315.
[82] Guttman F M, Lizin J, Robitaille P, *et al.* Survival of canine kidneys after treatment with dimethyl-sulfoxide, freezing at --80 degrees c, and thawing by microwave illumination. Cryobiology, 1977; 14(5): 559-567.
[83] Ma R, Ren S, Wang Z, *et al.* Electromagnetic rewarming for cryopreservation: a numerical comparison between multi-mode and single-mode electromagnetic cavity. Cryobiology, 2022; 109: 23.
[84] Martin Paul Robinson D E P. Rapid electromagnetic warming of cells and tissues. IEEE Transactions on Biomedical Engineering, 1999; 46(10): 1175-1181.
[85] Pan J, Shu Z, Ren S, *et al.* Determination of dielectric properties of cryoprotective agent solutions with a resonant cavity for the electromagnetic rewarming in cryopreservation. Biopreserv Biobank, 2017; 15(5): 404-409.
[86] Ren S, Shu Z, Peng J, *et al.* Rapid and uniform rewarming by single-mode electromagnetic resonance cavity: effect of sample shape. Cryobiology, 2021; 103: 188.
[87] Lewis J, Stoddart K, Reitinger V, *et al.* Molecular dynamics-informed optimization of cryoprotectant solutions for enhanced single-mode electromagnetic rewarming. Cryobiology, 2024; 117: 105091.
[88] Wang Z, Ren S, Shu Z, *et al.* Screening and optimization of cryoprotective agents(cpas) for electromagnetic heating of cryopreserved biomaterials. Cryobiology, 2022; 109: 16.
[89] Ren S, Shu Z, Wang Z, *et al.* Successful vitreous cryopreservation of rabbit jugular vein using magnetic nanoparticles enhanced single-mode electromagnetic resonance rewarming system. Cryobiology, 2021; 103: 173-174.
[90] Wang W. Design of low-noise low-power ecg amplifier circuit with high integration level. Journal of Physics Conference Series, 2023; 2649(1): 012062.
[91] Sun J, Wang W, Yue Q. Review on microwave-matter interaction fundamentals and efficient microwave-associated heating strategies. Materials(Basel), 2016; 9(4): 231.
[92] Han Z H, Rao J S, Gangwar L, *et al.* Vitrification and nanowarming enable long-term organ cryopreservation and life-sustaining kidney transplantation in a rat model. Nat Commun, 2023; 14(1): 3407.
[93] Gangwar L, Han Z, Scheithauer C, *et al.* Physical vitrification and nanowarming at human organ scale to enable cryopreservation. bioRxiv, 2024.
[94] Bischof J C, Oziri O J, Rao J S, *et al.* Scalable purification of iron oxide nanoparticles by tangential flow filtration for organ cryopreservation and transplantation. SPIE, 2025.
[95] Ye Z, Tai Y, Han Z, *et al.* Engineering magnetic nanoclusters for highly efficient heating in radio-frequency nanowarming. Nano Lett, 2024; 24(15): 4588-4594.
[96] Han Z, Gangwar L, Namsrai B-E, *et al.* Kidney tissue loading reduces the critical cooling and warming rates of vs55 and vmp cryoprotective solutions. Cryobiology, 2024; 117: 104977.